







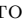








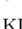







DRAFT VERSION JUNE 17, 2020
Typeset using L^AT_EX twocolumn style in AASTeX63

NGTS-11 b (TOI-1847 b): A transiting warm Saturn recovered from a *TESS* single-transit event

SAMUEL GILL ^{1,2} PETER J. WHEATLEY ^{1,2} BENJAMIN F. COOKE ² ANDRÉS JORDÁN ^{3,4} LOUISE D. NIELSEN ⁵
DANIEL BAYLISS ² DAVID R. ANDERSON ² JOSE I. VINES ⁶ MONIKA LENDL ^{5,7} JACK S. ACTON,⁸
DAVID J. ARMSTRONG ^{1,2} FRANÇOIS BOUCHY,⁵ RAFAEL BRAHM,^{3,4} EDWARD M. BRYANT,^{1,2} MATTHEW R. BURLEIGH ⁸
SARAH L. CASEWELL ⁸ PHILIPP EIGMÜLLER,⁹ NÉSTOR ESPINOZA ¹⁰ EDWARD GILLEN ^{11,12} MICHAEL R. GOAD,⁸
NOLAN GRIEVES,⁵ MAXIMILIAN N. GÜNTHER ^{13,14} THOMAS HENNING ¹⁵ MELISSA J. HOBSON ^{16,4} ALEISHA HOGAN,⁸
JAMES S. JENKINS,^{6,17} JAMES McCORMAC,² MAXIMILIANO MOYANO,¹⁸ HUGH P. OSBORN ^{19,13} DON POLLACCO ^{1,2}
DIDIER QUELOZ ¹¹ HEIKE RAUER,⁹ LIAM RAYNARD,⁸ FELIPE ROJAS,^{16,4} PAULA SARKIS,¹⁵ ALEXIS M. S. SMITH ⁹
MARCELO TALA PINTO,^{20,4} ROSANNA H. TILBROOK,⁸ STÉPHANE UDRY ⁵ CHRISTOPHER A. WATSON,²¹
RICHARD G. WEST ²

¹Centre for Exoplanets and Habitability, University of Warwick, Gibbet Hill Road, Coventry CV4 7AL, UK

²Department of Physics, University of Warwick, Gibbet Hill Road, Coventry CV4 7AL, UK

³Facultad de Ingeniería y Ciencias, Universidad Adolfo Ibáñez, Av. Diagonal las Torres 2640, Peñalolén, Santiago, Chile

⁴Millennium Institute for Astrophysics, Chile

⁵Observatoire astronomique de l'Université de Genève, Chemin des maillettes 51, 1290 Sauverny, Switzerland

⁶Departamento de Astronomía, Universidad de Chile, Camino El Observatorio 1515, Las Condes, Santiago, Chile

⁷Space Research Institute, Austrian Academy of Sciences, Schmiedlstr. 6, 8042 Graz, Austria

⁸School of Physics and Astronomy, University of Leicester, University Road, Leicester LE1 7RH, UK

⁹Institute of Planetary Research, German Aerospace Center, Rutherfordstrasse 2, 12489, Berlin, Germany

¹⁰Space Telescope Science Institute, 3700 San Martin Drive, Baltimore, MD 21218, USA

¹¹Astrophysics Group, Cavendish Laboratory, J.J. Thomson Avenue, Cambridge CB3 0HE, UK

¹²Winton Fellow

¹³Department of Physics and Kavli Institute for Astrophysics and Space Research, Massachusetts Institute of Technology, 70 Vassar Street, Cambridge, MA 02139, USA

¹⁴Juan Carlos Torres Fellow

¹⁵Max-Planck-Institut für Astronomie, Königstuhl 17, 69117 Heidelberg, Germany

¹⁶Instituto de Astrofísica, Facultad de Física, Pontificia Universidad Católica de Chile

¹⁷Centro de Astrofísica y Tecnologías Afines (CATA), Casilla 36-D, Santiago, Chile

¹⁸Instituto de Astronomía, Universidad Católica del Norte, Angamos 0610, 1270709 Antofagasta, Chile

¹⁹NCCR/PlanetS, Centre for Space & Habitability, University of Bern, Bern, Switzerland

²⁰Landessternwarte, Zentrum für Astronomie der Universität Heidelberg, Königstuhl 12, 69117 Heidelberg, Germany

²¹Astrophysics Research Centre, School of Mathematics and Physics, Queen's University Belfast, BT7 1NN, Belfast, UK

(Received June 1, 2019; Revised January 10, 2019; Accepted June 17, 2020)

Submitted to ApJL

ABSTRACT

We report the discovery of NGTS-11 b (=TOI-1847 b), a transiting Saturn in a 35.46-day orbit around a mid K-type star ($T_{\text{eff}}=5050 \pm 80$ K). We initially identified the system from a single-transit event in a *TESS* full-frame image light-curve. Following seventy-nine nights of photometric monitoring with an NGTS telescope, we observed a second full transit of NGTS-11 b approximately one year after the *TESS* single-transit event. The NGTS transit confirmed the parameters of the transit signal and restricted the orbital period to a set of 13 discrete periods. We combined our transit detections with precise radial velocity measurements to determine the true orbital period and measure the mass of

the planet. We find NGTS-11 b has a radius of $0.817 \pm_{0.032}^{0.028} R_{\text{Jup}}$, a mass of $0.344 \pm_{0.073}^{0.092} M_{\text{Jup}}$, and an equilibrium temperature of just $435 \pm_{32}^{34}$ K, making it one of the coolest known transiting gas giants. NGTS-11 b is the first exoplanet to be discovered after being initially identified as a *TESS* single-transit event, and its discovery highlights the power of intense photometric monitoring in recovering longer-period transiting exoplanets from single-transit events.

Keywords: planets and satellites: detection

1. INTRODUCTION

Wide-field photometric surveys have uncovered a large population of transiting exoplanets around bright stars (e.g. Bakos et al. 2004; Pollacco et al. 2006; Borucki et al. 2010), providing key opportunities to measure precise planetary radii and densities, constrain bulk composition, and to characterise planetary atmospheres (e.g. Seager & Mallén-Ornelas 2003; Fortney et al. 2007; Sing et al. 2016). However, the transit geometry imposes a strong selection bias for close-in orbits, and only a handful of well-characterised transiting exoplanets are known with orbital periods longer than about 30 days. This limits our characterisation of the wider exoplanet population, as well as its evolution through planetary migration (e.g. Nottale et al. 2004; Jones et al. 2004; Alibert et al. 2013). It also prevents us from using transits to characterise exoplanets in the habitable zone (Kasting et al. 1993; Kopparapu et al. 2013), except around very late-type host stars (e.g. Gillon et al. 2017).

The extremely wide field of the *TESS* survey (Ricker et al. 2015) is providing many new exoplanet candidates around bright stars. Longer-period planets can be confirmed at high ecliptic latitudes, where *TESS* monitors stars for up to one year (e.g. Eisner et al. 2020; Dalba et al. 2020). However, with an observing baseline of only 27 days across most of the sky, *TESS* typically detects only a single transit for longer-period planets (Cooke et al. 2018; Villanueva et al. 2019). Follow-up of these single transit events provide the opportunity to discover and characterise many more longer-period planets (Yee & Gaudi 2008; Yao et al. 2019). However, a single-transit event provides only a weak constraint on the orbital period of the planet (Osborn et al. 2016; Sandford et al. 2019), and so follow-up observations designed to confirm the exoplanet are expensive: whether aiming to detect additional transits, or to detect the radial velocity variations of the host star.

The NGTS project (Wheatley et al. 2018) has commenced a program to follow-up *TESS* single-transit event candidates, and has already discovered three longer-period, low-mass eclipsing binary systems: TIC-238855958 (Gill et al. 2020a), TOI-222 (Lendl et al. 2020), and TIC-231005575 (Gill et al. 2020b).

In this letter we present the first discovery of an exoplanet based on a single-transit event from *TESS*. We show how an observing strategy focusing on detecting a second transit, in this case with NGTS, enables longer-period planets to be confirmed and characterised using a very modest number of radial velocity measurements.

2. OBSERVATIONS AND ANALYSIS

2.1. *TESS* single transit detection

Using light curves produced from the *TESS* calibrated full-frame images by Oelkers & Stassun (2018), we conducted a systematic search for single-transit events using the procedure described by Gill et al. (2020a).

The K-dwarf TIC-54002556 (hereafter NGTS-11, $T = 11.62$, properties in Table 1) was observed at 30-minute cadence with *TESS* Camera 1 during Sector 3 of the mission (2018 September 20 – 2018 October 18). NGTS-11 was not selected for *TESS* 2-minute cadence observations, so does not have a light curve from the SPOC pipeline.

We identified a promising single-transit event from NGTS-11 approximately nine days into Sector 3, at JD 2458390.7, with a transit width of 4 h and depth of 1 percent (shown in top panel of Fig. 1). We inspected the individual *TESS* calibrated full-frame images for asteroids and any other anomalies. We also searched for blended objects in Gaia DR2 (Gaia Collaboration et al. 2018) and checked for known nearby exoplanets or eclipsing binaries that might be the source of the transit event. We found no reason to believe this single-transit candidate was a false-positive.

Having identified NGTS-11 as hosting a viable exoplanet candidate, we created a higher quality *TESS* light curve from the *TESS* calibrated full-frame images by carefully selecting source and background pixel apertures in order to minimise blending with neighbouring objects. Background pixels were selected from a 15×15 pixel median master frame using an iterative sigma-clipping process. Source pixels were selected from a central 7×7 pixel region where median pixel counts exceeded the background level by 100 times the standard deviation in the background. To exclude source pixels contaminated by neighbouring objects, we also required a monotonic decrease in counts with distance from the

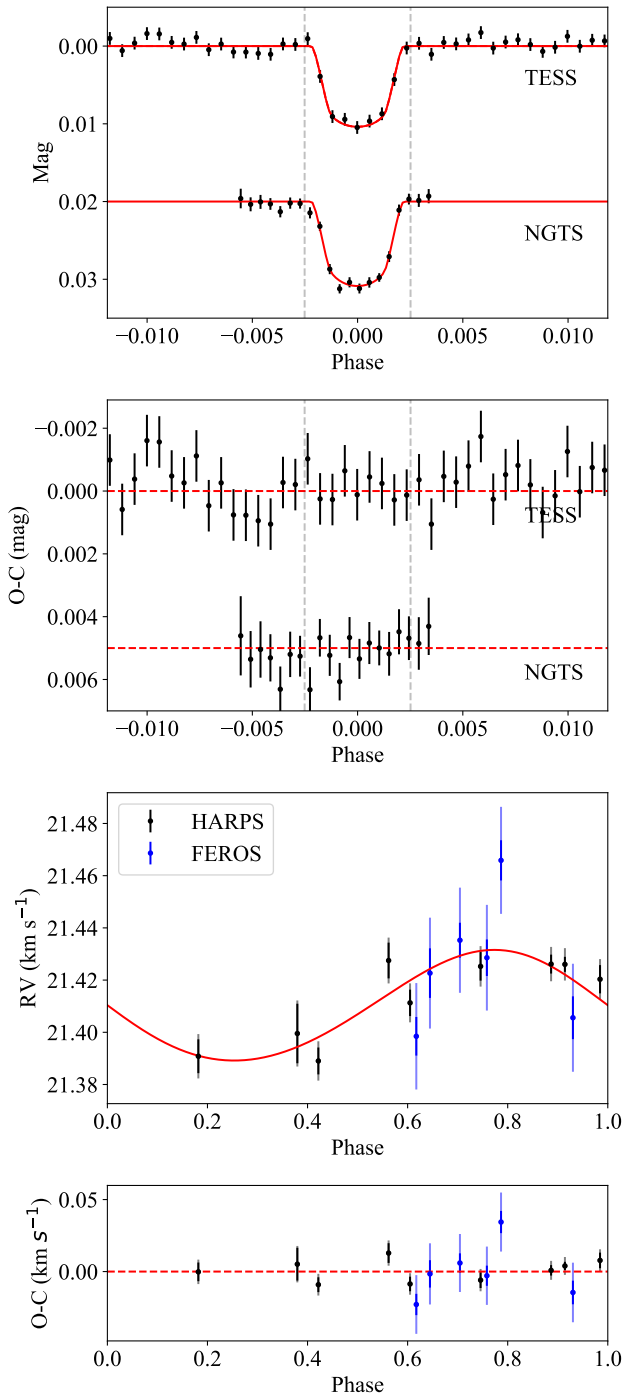


Figure 1. Our best-fitting model to the photometric and radial velocity observations of NGTS-11. Upper panel shows the transit photometry of *TESS* and NGTS with the model in red. Dashed vertical grey lines indicate start of ingress and end of egress. Photometric residuals are shown in the upper-middle panel. NGTS photometry has been binned to 30 min for plotting purposes, but was fitted at the full 13 s time resolution. The lower panels show the radial velocity observations and residuals from FEROS (blue) and HARPS (black) along with our best-fitting model (red). Semi-transparent error bars represent uncertainties with jitter values added in quadrature.

target position. The final source aperture included 19 pixels.

These apertures better exclude fainter, nearby companions TIC-54002560 ($48.51''$; $T = 14.28$) and TIC-54002559 ($56.41''$; $T = 14.51$). Frames with a quality flag larger than 0 were rejected, and the light curve was detrended using a median filter of width 10.5 h. The resulting *TESS* light curve around the time of the transit is shown in Fig. 1, and this was used for the remainder of this work.

2.2. A second transit with NGTS

We used the NGTS facility (Wheatley et al. 2018) located at the ESO Paranal Observatory in Chile to monitor NGTS-11 photometrically, searching for additional transits. NGTS was designed specifically for very high precision photometry of exoplanet transits, and it is thus well suited to photometric follow-up of *TESS* single-transit candidates (Wheatley et al. 2018). We started monitoring NGTS-11 with a single NGTS telescope on the night of 2019 August 11. We observed each subsequent night with 10 s exposures whenever the target was above an elevation of 30 deg and weather conditions allowed. The images were reduced to light curves each day using the on-site NGTS real-time aperture photometry pipeline described by Bryant et al. (2020).

We used the template matching algorithm described by Gill et al. (2020a,b) to search the NGTS light curve for additional transit events. This involved using a model fit to the *TESS* transit as a template, which was placed at each possible transit epoch within the NGTS light curve and the improvement in log-likelihood calculated ($\Delta \log \mathcal{L} = -\Delta \chi^2/2$). From empirical injection tests, we conservatively estimated that a significant template match would be consistent with $\Delta \log \mathcal{L} > 50$. We observed NGTS-11 for 79 nights (105 642 exposures) before a second transit event was detected ($\Delta \log \mathcal{L} = 364$) on the UT night of 24 October 2019. The transit event was centred at JD 2458780.712, which is 390 days after the initial *TESS* single-transit. The NGTS transit detection is plotted in the top panel of Fig. 1.

2.3. Photometric constraints on orbital period

We measured the precise separation of the *TESS* and NGTS transit detections using a joint transit fit to both light curves, finding $\Delta T = 390.0082 \pm 0.0032$ days. The orbital period of the companion to NGTS-11 must be an integer fraction of this duration. We label these candidate periods as $P_n = (390.0082/n)$ where n is an integer. These candidate periods are indicated with vertical lines in Figure 2.

All candidate periods beyond P_{18} were ruled out by the *TESS* data, since additional transits would have

Table 1. Catalogued, measured and derived properties of NGTS-11 and NGTS-11 b.

Catalogue data		Model parameters	
TIC ID	TIC-54002556	T_0 (BJD-TDB)	2458390.7043 ± 0.0016
R.A.	$01^{\text{h}}34'05.15''$	P (d)	35.45533 ± 0.00019
decl.	$-14^{\circ}25'08.9''$	R_*/a	$0.0183 \pm_{0.0025}^{0.0029}$
G	12.1895 ± 0.0002	R_p/R_*	$0.1010 \pm_{0.0037}^{0.0030}$
BP	12.6725 ± 0.0012	b	$0.81 \pm_{0.10}^{0.13}$
RP	11.5707 ± 0.0011	$h_{1,TESS}$	$0.7406 \pm_{0.0030}^{0.0030}$
pmRA (mas yr ⁻¹)	11.168 ± 0.099	$h_{2,TESS}$	$0.427 \pm_{0.046}^{0.046}$
pmDec (mas yr ⁻¹)	14.047 ± 0.049	$h_{1,NGTS}$	$0.7144 \pm_{0.0030}^{0.0031}$
Parallax (mas)	5.223 ± 0.048	$h_{2,NGTS}$	$0.442 \pm_{0.046}^{0.043}$
<i>TESS</i> (T)	11.624 ± 0.006	$l_{3,TESS}$	$0.051 \pm_{0.034}^{0.048}$
APASS9 (B)	13.308 ± 0.035	K_* (km s ⁻¹)	$0.0212 \pm_{0.0041}^{0.0046}$
APASS9 (V)	12.456 ± 0.080	$\sqrt{e} \sin \omega$	$0.13 \pm_{0.28}^{0.26}$
APASS9 (g')	12.852 ± 0.038	$\sqrt{e} \cos \omega$	$0.19 \pm_{0.22}^{0.16}$
APASS9 (r')	12.127 ± 0.012	γ (km s ⁻¹)	$21.4094 \pm_{0.0028}^{0.0029}$
APASS9 (i')	11.864 ± 0.083	$\Delta\gamma_{\text{FEROS}}$ (km s ⁻¹)	$-0.042 \pm_{0.010}^{0.010}$
2MASS (J)	10.855 ± 0.025	Derived planet properties	
2MASS (H)	10.401 ± 0.023	M_p (M_{Jup})	$0.344 \pm_{0.073}^{0.092}$
2MASS (K _s)	10.315 ± 0.025	R_p (R_{Jup})	$0.817 \pm_{0.032}^{0.028}$
Stellar parameters		a (au)	$0.2010 \pm_{0.0022}^{0.0021}$
T_{eff} (K)	5050 ± 80	e	$0.13 \pm_{0.09}^{0.10}$
[Fe/H] (dex)	0.22 ± 0.08	ω (deg)	$32 \pm_{76}^{53}$
$\log g_*$ (dex)	4.5 ± 0.1	i (deg)	$89.16 \pm_{0.29}^{0.20}$
$v \sin i$ (km s ⁻¹)	1.1 ± 0.8	T_{dur} (hr)	$3.59 \pm_{0.37}^{0.18}$
M_* (M_{\odot})	0.862 ± 0.028	g_p (m s ⁻²)	$14.1 \pm_{3.4}^{5.3}$
R_* (R_{\odot})	0.832 ± 0.013	T_{eq} (K)	$435 \pm_{32}^{34}$
ρ_* (ρ_{\odot})	1.496 ± 0.085	ρ_p (g cm ⁻³)	$0.78 \pm_{0.17}^{0.21}$
Age (Gyr)	3.9 ± 1.6	H_p (km)	$141 \pm_{51}^{74}$

been detected. Similarly, five candidate periods (P_{10} , P_{13} , P_{14} , P_{15} and P_{17}) were ruled out by the NGTS photometric monitoring as well as additional observations on 2019 November 22 and 2019 December 1 (red dashed vertical lines in Figure 2). This left just 13 candidate orbital periods (green dashed vertical lines in Figure 2).

2.4. Radial velocity measurements

Following the NGTS transit detection, we immediately began radial-velocity follow-up using the CORALIE fiber-fed Échelle spectrograph installed on the 1.2-m Leonard Euler telescope at the ESO La Silla Observatory (Queloz et al. 2001). We made three 600 s observations of NGTS-11 over 54 days (2019 October 29, November 28, and December 25), the first just 5 days after the NGTS transit detection. The spectra were reduced using the CORALIE standard reduction pipeline, with radial velocity measurements derived using the cross-correlation technique and a numerical G2 mask. The radial velocities had no variation above 80 m s^{-1}

showing that the transiting companion is unlikely to be a low-mass star.

This motivated an additional nine 1800 s radial velocity measurements spanning 63 days with the HARPS spectrograph ($R = 115000$) on the 3.6-m ESO telescope (Pepe et al. 2002) and six measurements spanning 11 days with the FEROS spectrograph ($R = 48000$) on the MPG/ESO 2.2-m Telescope (Kaufer et al. 1999). The FEROS data were reduced with the CERES pipeline (Brahm et al. 2017). These data are plotted in the lower panels of Figure 1.

2.5. Stellar properties

We used our HARPS spectra to determine the properties of the host star NGTS-11. The individual spectra were shifted to the laboratory frame of reference and co-added to produce a combined spectrum with a signal-to-noise ratio of 44. We used ISPEC (Blanco-Cuaresma et al. 2014) to synthesise models using the radiative transfer code SPECTRUM (Gray 1999), MARCS model atmospheres (Gustafsson et al. 2008), and version 5 of

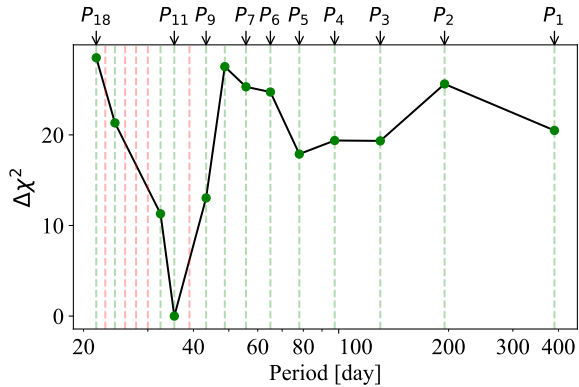


Figure 2. The relative goodness-of-fit for different candidate orbital periods from our joint fits to the *TESS* and NGTS transit detections and radial velocity measurements of NGTS-11 (described in Section 2.6). Priors were used to constrain each fit to orbital periods around those allowed by the *TESS* and NGTS photometry (green dashed lines). Orbital periods excluded by NGTS observations are marked in red (see Section 2.3). Our best fit is to P_{11} ($= 390.0082/11 = 35.46$ days).

the GAIA ESO survey (GES) atomic line list within ISPEC with solar abundances from Asplund et al. (2009). We used the $H\alpha$, $NaID$, and $MgIb$ lines to determine the stellar effective temperature, T_{eff} , and surface gravity, $\log g$. We used individual FeI and FeII lines to determine metallicity, $[Fe/H]$, and the rotational broadening projected into the line of sight, $v \sin i$. Values of macroturbulence and microturbulence were calculated using equations 5.10 and 3.1 respectively from Doyle (2015).

We used the method described in Gill et al. (2020a) to determine the mass, radius, and age of NGTS-11. This method uses Gaia magnitudes and parallax (Gaia Collaboration et al. 2018) along with T_{eff} and $[Fe/H]$ from our spectroscopy to determine the best-fitting stellar parameters with respect to MESA models (Dotter 2016; Choi et al. 2016).

The results of our analysis are presented in Table 1. We find that NGTS-11 is a mid K-dwarf star ($T_{\text{eff}}=5050 \pm 80$ K) with super-Solar metallicity of $[Fe/H]=0.22 \pm 0.08$.

2.6. Orbital period and planet properties

In order to determine the true orbital period of NGTS-11 b, as well as its physical properties, we carried out joint fits of our transit light curves (*TESS* and NGTS) and radial velocity data (HARPS and FEROS) at each of the candidate orbital periods allowed by the photometry (see Section 2.3 and Figure 2).

A perfect minimisation algorithm would explore the whole parameter space in a single fit, finding each of the thirteen orbital periods allowed by the photome-

try for itself. However, the χ^2 minima are narrow and widely spaced, and this approach is not efficient in practice. Instead, we explored each minimum with a separate MCMC run, using a uniform prior that selected the period alias in question, but did not define the period itself. Figure 2 shows the best χ^2 from each of these 13 runs, mapping the depth of each χ^2 minimum.

Our model has 17 free parameters, with best-fitting values presented in Table 1, and the best-fitting model shown in Figure 1. In addition to the orbital period, P , these include T_0 , the *TESS* transit epoch, R_*/a , R_p/R_* , and the transit impact parameter, b , where R_* is the radius of the star, R_p is the radius of the planet, and a is the orbital separation. For the *TESS* and NGTS transit data we also fit for the out-of-transit magnitude offsets, as well as the decorrelated limb-darkening parameters h_1 and h_2 from Maxted (2018). We employed Gaussian priors on h_1 and h_2 for each instrument interpolated from Maxted (2018) using stellar atmospheric parameters from Section 2.5. These priors dominate the posterior distributions for h_1 and h_2 . In our initial fits we found that the *TESS* transit was slightly shallower than the NGTS transit, which we ascribe to residual blending with the neighbouring stars mentioned in Section 2.1. We therefore introduced a parameter to allow for third light in the *TESS* light curve, $l_{3,TESS}$. Instead of fitting directly for eccentricity, e , and the argument of periastron, ω , we use the decorrelated parameters $\sqrt{e} \sin \omega$ and $\sqrt{e} \cos \omega$, which perform better at low eccentricities (Ford 2006). Our model also includes the radial velocity semi-amplitude of the host star, K_* , and the system velocity, γ .

To account for different zero-points between HARPS and FEROS we also include a radial velocity offset for the FEROS data with respect to HARPS, $\Delta\gamma_{\text{FEROS}}$. To allow for astrophysical and/or instrumental noise not included in the formal radial velocity uncertainties we add a radial velocity jitter term in quadrature to the formal radial velocity uncertainties. To obtain a spectroscopic reduced χ^2 of unity, jitter terms of 5.5 m s^{-1} for HARPS and 19.0 m s^{-1} for FEROS are required. These jitter terms are in line with expectations for these instruments and a star of this brightness (e.g. Raynard et al. 2018; Hartman et al. 2019, 2020). The bisector span shows no significant correlation with radial velocity.

We used EMCEE (Foreman-Mackey et al. 2013) to explore the parameter space around each candidate orbital period using the likelihood function $\mathcal{L}(\mathbf{d}|\mathbf{m}) = \exp(-\chi^2/2)$. We initiated 36 Markov chains and generated 100000 trial steps. We discarded the first 50000 as burn-in and visually confirmed the sampler had converged. Median parameter values for the best-fitting

model at $P_{11} = 35.46$ days are reported in Table 1, and the uncertainties are estimated using the 16th and 84th percentiles of the cumulative posterior distributions.

Figure 2 shows how the best-fitting χ^2 depends on the orbital period alias. Our best fit is to $P_{11} = 35.46$ days, and the next best fitting candidate period (P_{12}) has $\Delta\chi^2 = 11.3$, which makes it more than 250 times less probable. It is important to understand that the fits to the different period aliases in Fig. 2 are effectively a single fit (with identical model and free parameters) exploring a complex χ^2 space with multiple widely-spaced minima (at the periods allowed by the photometry in Sect. 2.3). The $\Delta\chi^2$ plotted is identical to ΔBIC (Bayesian information criterion).

Our best fitting model is shown in Figure 1, and the corresponding parameters are listed in Table 1. This shows NGTS-11 b to be an exoplanet with mass and radius very similar to Saturn (see Figure 3).

3. DISCUSSION AND CONCLUSIONS

Following-up a single-transit event identified in our *TESS* light curve of the K-dwarf NGTS-11, we have detected a second transit event with NGTS. Combined with radial velocity follow-up with CORALIE, HARPS, and FEROS, these transit detections show that the companion object is an exoplanet with mass and radius similar to Saturn. The planet has a 35.46 day orbit that is marginally eccentric. NGTS-11 b is the first exoplanet to be confirmed after initially being identified as a *TESS* single-transit event. At our request, NGTS-11 b has also been designated TOI-1847 b.

Figure 3 puts NGTS-11 b into context with the wider population of well-characterised exoplanets. The planet radius is not inflated compared to the solar system giants, as expected for a wide-separation planet (Laughlin et al. 2011; Thorngren & Fortney 2018; Sestovic et al. 2018), and its composition is consistent with that of Saturn. NGTS-11 b has a surface gravity, g_p , of $14.1 \pm_{3.4}^{5.3} \text{ m s}^{-2}$, calculated using the method of Southworth et al. (2007). Assuming an albedo similar to Saturn (0.342; Hanel et al. 1983), we calculate an equilibrium temperature of only $435 \pm_{32}^{34} \text{ K}$. Since the host star is a K-dwarf, this equilibrium temperature is lower even than some longer-period planets with F- and G-type hosts. In fact NGTS-11 b is one of just a handful of transiting gas giant planets with an equilibrium temperature $< 500 \text{ K}$. This makes NGTS-11 b an interesting prospect for transmission spectroscopy to study an atmosphere that is much cooler than the typically-studied hot Jupiters, which have equilibrium temperatures of 1000–2500 K (e.g. Sing et al. 2016). Assuming a Saturn-

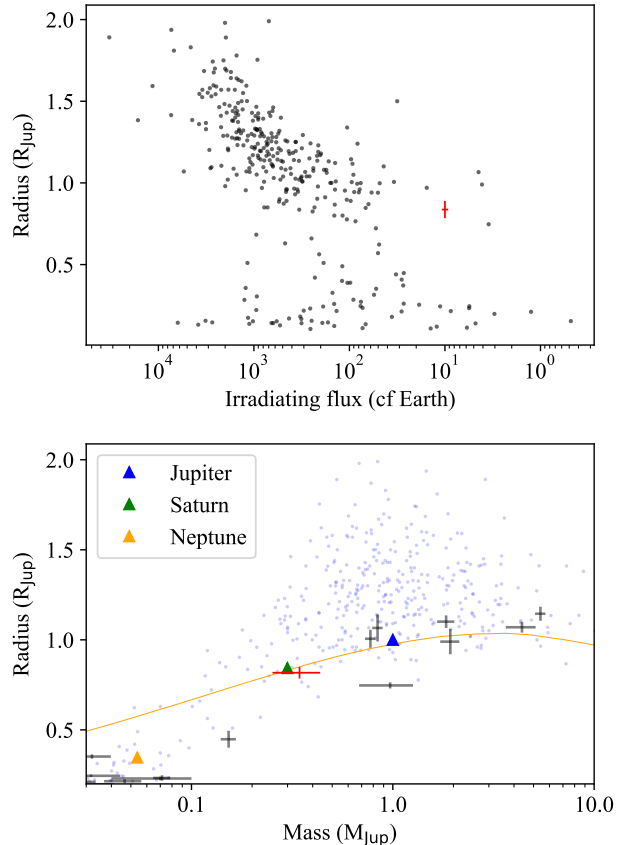


Figure 3. Upper panel: Radius-irradiation diagram of well-characterised transiting exoplanets (mass to better than 50% precision and radius to better than 20%; exoplanetarchive.ipac.caltech.edu, accessed 04/30/2020). NGTS-11 b is indicated in red. Lower panel: Mass-radius diagram for giant exoplanets from the same sample. Planets with orbital periods longer than 30 days are plotted in black, those with periods shorter than 30 days in blue. NGTS-11 b is again represented with a red star and solar system giants are indicated with triangles. The orange line shows a theoretical mass-radius relation for a cold hydrogen/helium exoplanet (Seager et al. 2007).

like atmospheric composition (2.07 g mole^{-1})¹ we estimate an atmospheric scale height, H_p , of $141 \pm_{51}^{74} \text{ km}$, which may make it a viable target for transmission spectroscopy. The long baseline between the two transit detections already provides good precision for predicting future transits. For instance, the uncertainty in the timing of transit events in 2025 is only 28 minutes.

It is important to note that we have been able to determine the mass and radius of this relatively long-period exoplanet with a very modest number of radial velocity measurements (nine with HARPS and six with FEROS).

¹ <https://nssdc.gsfc.nasa.gov>

The detection of the second transit with NGTS was crucial in tightly constraining the possible orbital periods, and this serves to demonstrate the value of intense photometric monitoring in following-up single transit events. Without this second transit detection we would have required many more radial velocity measurements in order to confirm the planet, determine its orbital period, and measure its mass (e.g. Díaz et al. 2020). The strategy of large investments of photometric follow-up with instruments such as NGTS thereby allows efficient confirmation of single-transit events without adding to the considerable pressure on high-precision radial velocity instruments. This highlights the power of high-precision ground-based photometric facilities in revealing longer period transiting exoplanets that *TESS* alone cannot discover.

ACKNOWLEDGMENTS

The NGTS facility is operated by the consortium institutes with support from the UK Science and Technology Facilities Council (STFC) under projects ST/M001962/1 and ST/S002642/1.

This paper includes data collected with the *TESS* mission, obtained from the MAST data archive at the Space Telescope Science Institute (STScI). Funding for the *TESS* mission is provided by the NASA Explorer Program. STScI is operated by the Association of Universities for Research in Astronomy, Inc., under NASA contract NAS 526555.

Based on observations made with ESO Telescopes at the La Silla Paranal Observatory under programme IDs 0104.C – 0413 (PI RB), 0104.C – 0588 (PI FB), Opticon:2019A/037 (PI DB), and CNTAC: 0104.A – 9012 (PI JIV).

The contributions at the University of Warwick by PJW, RGW, DLP, DJA, DRA, SG, and TL have been supported by STFC through consolidated grants ST/L000733/1 and ST/P000495/1. DJA acknowledges

support from the STFC via an Ernest Rutherford Fellowship (ST/R00384X/1). Contributions at the University of Geneva by FB, LN, ML, OT, and SU were carried out within the framework of the National Centre for Competence in Research “PlanetS” supported by the Swiss National Science Foundation (SNSF). The contributions at the University of Leicester by MRG and MRB have been supported by STFC through consolidated grant ST/N000757/1. SLC acknowledges support from the STFC via an Ernest Rutherford Fellowship (ST/R003726/1). This project has received funding from the European Union’s Horizon 2020 research and innovation programme under grant agreement No 730890. AJ, RB and MH acknowledge support from project IC120009 “Millennium Institute of Astrophysics (MAS)” of the Millenium Science Initiative, Chilean Ministry of Economy. AJ acknowledges additional support from FONDECYT project 1171208. RB acknowledges support from FONDECYT Post-doctoral Fellowship Project 3180246. JSJ is supported by funding from Fondecyt through grant 1161218 and partial support from CATA-Basal (PB06, Conicyt). MNG acknowledges support from the Juan Carlos Torres Fellowship. ACh acknowledges the support of the DFG priority program SPP 1992 “Exploring the Diversity of Extrasolar Planets” (RA 714/13-1). JIV acknowledges support of CONICYT-PFCHA/Doctorado Nacional-21191829. EG gratefully acknowledges support from the David and Claudia Harding Foundation in the form of a Winton Exoplanet Fellowship. TH acknowledges support from the European Research Council under the Horizon 2020 Framework Program via the ERC Advanced Grant Origins 83 24 28. This research has made use of NASA’s Astrophysics Data System Bibliographic Services and the SIMBAD database, operated at CDS, Strasbourg, France. This research made use of *Astropy*,² a community-developed core Python package for Astronomy (The *Astropy Collaboration et al.* 2018).

REFERENCES

- Alibert, Y., Carron, F., Fortier, A., et al. 2013, *A&A*, 558, A109, doi: [10.1051/0004-6361/201321690](https://doi.org/10.1051/0004-6361/201321690)
- Asplund, M., Grevesse, N., Sauval, A. J., & Scott, P. 2009, *ARA&A*, 47, 481, doi: [10.1146/annurev.astro.46.060407.145222](https://doi.org/10.1146/annurev.astro.46.060407.145222)
- Bakos, G., Noyes, R. W., Kovács, G., et al. 2004, *PASP*, 116, 266, doi: [10.1086/382735](https://doi.org/10.1086/382735)
- Blanco-Cuaresma, S., Soubiran, C., Jofré, P., & Heiter, U. 2014, in *Astronomical Society of India Conference Series*, Vol. 11, *Astronomical Society of India Conference Series*, 85–91. <https://arxiv.org/abs/1312.4545>
- Borucki, W. J., Koch, D., Basri, G., et al. 2010, *Science*, 327, 977, doi: [10.1126/science.1185402](https://doi.org/10.1126/science.1185402)
- Brahm, R., Jordán, A., & Espinoza, N. 2017, *PASP*, 129, 034002, doi: [10.1088/1538-3873/aa5455](https://doi.org/10.1088/1538-3873/aa5455)

² <http://www.astropy.org>

- Bryant, E. M., Bayliss, D., McCormac, J., et al. 2020, arXiv e-prints, arXiv:2004.07589.
<https://arxiv.org/abs/2004.07589>
- Choi, J., Dotter, A., Conroy, C., et al. 2016, *ApJ*, 823, 102, doi: [10.3847/0004-637X/823/2/102](https://doi.org/10.3847/0004-637X/823/2/102)
- Cooke, B. F., Pollacco, D., West, R., McCormac, J., & Wheatley, P. J. 2018, *A&A*, 619, A175, doi: [10.1051/0004-6361/201834014](https://doi.org/10.1051/0004-6361/201834014)
- Dalba, P. A., Gupta, A. F., Rodriguez, J. E., et al. 2020, *AJ*, 159, 241, doi: [10.3847/1538-3881/ab84e3](https://doi.org/10.3847/1538-3881/ab84e3)
- Díaz, M. R., Jenkins, J. S., Feng, F., et al. 2020, arXiv e-prints, arXiv:2003.10319.
<https://arxiv.org/abs/2003.10319>
- Dotter, A. 2016, *ApJS*, 222, 8, doi: [10.3847/0067-0049/222/1/8](https://doi.org/10.3847/0067-0049/222/1/8)
- Doyle, A. P. 2015, PhD thesis, Keele University
- Eisner, N. L., Barragán, O., Aigrain, S., et al. 2020, *MNRAS*, 494, 750, doi: [10.1093/mnras/staa138](https://doi.org/10.1093/mnras/staa138)
- Ford, E. B. 2006, *ApJ*, 642, 505, doi: [10.1086/500802](https://doi.org/10.1086/500802)
- Foreman-Mackey, D., Hogg, D. W., Lang, D., & Goodman, J. 2013, *PASP*, 125, 306, doi: [10.1086/670067](https://doi.org/10.1086/670067)
- Fortney, J. J., Marley, M. S., & Barnes, J. W. 2007, *ApJ*, 659, 1661, doi: [10.1086/512120](https://doi.org/10.1086/512120)
- Gaia Collaboration, Brown, A. G. A., Vallenari, A., et al. 2018, *A&A*, 616, A1, doi: [10.1051/0004-6361/201833051](https://doi.org/10.1051/0004-6361/201833051)
- Gill, S., Bayliss, D., Cooke, B. F., et al. 2020a, *MNRAS*, 491, 1548, doi: [10.1093/mnras/stz3212](https://doi.org/10.1093/mnras/stz3212)
- Gill, S., Cooke, B. F., Bayliss, D., et al. 2020b, arXiv e-prints, arXiv:2002.09311.
<https://arxiv.org/abs/2002.09311>
- Gillon, M., Triaud, A. H. M. J., Demory, B.-O., et al. 2017, *Nature*, 542, 456, doi: [10.1038/nature21360](https://doi.org/10.1038/nature21360)
- Gray, R. O. 1999, SPECTRUM: A stellar spectral synthesis program. <http://ascl.net/9910.002>
- Gustafsson, B., Edvardsson, B., Eriksson, K., et al. 2008, *A&A*, 486, 951, doi: [10.1051/0004-6361:200809724](https://doi.org/10.1051/0004-6361:200809724)
- Hanel, R. A., Conrath, B. J., Kunde, V. G., Pearl, J. C., & Pirraglia, J. A. 1983, *Icarus*, 53, 262, doi: [10.1016/0019-1035\(83\)90147-1](https://doi.org/10.1016/0019-1035(83)90147-1)
- Hartman, J. D., Bakos, G. Á., Bayliss, D., et al. 2019, *AJ*, 157, 55, doi: [10.3847/1538-3881/aaf8b6](https://doi.org/10.3847/1538-3881/aaf8b6)
- Hartman, J. D., Jordán, A., Bayliss, D., et al. 2020, *AJ*, 159, 173, doi: [10.3847/1538-3881/ab7821](https://doi.org/10.3847/1538-3881/ab7821)
- Jones, H. R. A., Butler, R. P., Tinney, C. G., et al. 2004, *Astronomical Society of the Pacific Conference Series*, Vol. 321, HD10647 and the Distribution of Exoplanet Properties with Semi-major Axis (ASP Conference Proceedings), 298
- Kasting, J. F., Whitmire, D. P., & Reynolds, R. T. 1993, *Icarus*, 101, 108, doi: [10.1006/icar.1993.1010](https://doi.org/10.1006/icar.1993.1010)
- Kaufer, A., Stahl, O., Tubbesing, S., et al. 1999, *The Messenger*, 95, 8
- Kopparapu, R. K., Ramirez, R., Kasting, J. F., et al. 2013, *ApJ*, 765, 131, doi: [10.1088/0004-637X/765/2/131](https://doi.org/10.1088/0004-637X/765/2/131)
- Laughlin, G., Crismani, M., & Adams, F. C. 2011, *ApJL*, 729, L7, doi: [10.1088/2041-8205/729/1/L7](https://doi.org/10.1088/2041-8205/729/1/L7)
- Lendl, M., Bouchy, F., Gill, S., et al. 2020, *MNRAS*, 492, 1761, doi: [10.1093/mnras/stz3545](https://doi.org/10.1093/mnras/stz3545)
- Maxted, P. F. L. 2018, *A&A*, 616, A39, doi: [10.1051/0004-6361/201832944](https://doi.org/10.1051/0004-6361/201832944)
- Nottale, L., Ceccolini, D., da Rocha, D., et al. 2004, *Astronomical Society of the Pacific Conference Series*, Vol. 321, Structuring of the Semi-Major Axis and Eccentricity Distributions of Exoplanets (ASP Conference Proceedings), 355
- Oelkers, R. J., & Stassun, K. G. 2018, *AJ*, 156, 132, doi: [10.3847/1538-3881/aad68e](https://doi.org/10.3847/1538-3881/aad68e)
- Osborn, H. P., Armstrong, D. J., Brown, D. J. A., et al. 2016, *MNRAS*, 457, 2273, doi: [10.1093/mnras/stw137](https://doi.org/10.1093/mnras/stw137)
- Pepe, F., Mayor, M., Rupprecht, G., et al. 2002, *The Messenger*, 110, 9
- Pollacco, D. L., Skillen, I., Collier Cameron, A., et al. 2006, *PASP*, 118, 1407, doi: [10.1086/508556](https://doi.org/10.1086/508556)
- Queloz, D., Henry, G. W., Sivan, J. P., et al. 2001, *A&A*, 379, 279, doi: [10.1051/0004-6361:20011308](https://doi.org/10.1051/0004-6361:20011308)
- Raynard, L., Goad, M. R., Gillen, E., et al. 2018, *MNRAS*, 481, 4960, doi: [10.1093/mnras/sty2581](https://doi.org/10.1093/mnras/sty2581)
- Ricker, G. R., Winn, J. N., Vanderspek, R., et al. 2015, *Journal of Astronomical Telescopes, Instruments, and Systems*, 1, 014003, doi: [10.1117/1.JATIS.1.1.014003](https://doi.org/10.1117/1.JATIS.1.1.014003)
- Sandford, E., Espinoza, N., Brahm, R., & Jordán, A. 2019, *MNRAS*, 489, 3149, doi: [10.1093/mnras/stz2348](https://doi.org/10.1093/mnras/stz2348)
- Seager, S., Kuchner, M., Hier-Majumder, C. A., & Militzer, B. 2007, *ApJ*, 669, 1279, doi: [10.1086/521346](https://doi.org/10.1086/521346)
- Seager, S., & Mallén-Ornelas, G. 2003, *ApJ*, 585, 1038, doi: [10.1086/346105](https://doi.org/10.1086/346105)
- Sestovic, M., Demory, B.-O., & Queloz, D. 2018, *A&A*, 616, A76, doi: [10.1051/0004-6361/201731454](https://doi.org/10.1051/0004-6361/201731454)
- Sing, D. K., Fortney, J. J., Nikolov, N., et al. 2016, *Nature*, 529, 59, doi: [10.1038/nature16068](https://doi.org/10.1038/nature16068)
- Southworth, J., Wheatley, P. J., & Sams, G. 2007, *MNRAS*, 379, L11, doi: [10.1111/j.1745-3933.2007.00324.x](https://doi.org/10.1111/j.1745-3933.2007.00324.x)
- The Astropy Collaboration, Price-Whelan, A. M., Sipőcz, B. M., et al. 2018, *AJ*, 156, 123, doi: [10.3847/1538-3881/aabc4f](https://doi.org/10.3847/1538-3881/aabc4f)
- Thorngren, D. P., & Fortney, J. J. 2018, *AJ*, 155, 214, doi: [10.3847/1538-3881/aaba13](https://doi.org/10.3847/1538-3881/aaba13)
- Villanueva, Steven, J., Dragomir, D., & Gaudi, B. S. 2019, *AJ*, 157, 84, doi: [10.3847/1538-3881/aaf85e](https://doi.org/10.3847/1538-3881/aaf85e)

Wheatley, P. J., West, R. G., Goad, M. R., et al. 2018,
MNRAS, 475, 4476, doi: [10.1093/mnras/stx2836](https://doi.org/10.1093/mnras/stx2836)

Yao, X., Pepper, J., Gaudi, B. S., et al. 2019, The
Astronomical Journal, 157, 37,
doi: [10.3847/1538-3881/aaf23c](https://doi.org/10.3847/1538-3881/aaf23c)
Yee, J. C., & Gaudi, B. S. 2008, ApJ, 688, 616,
doi: [10.1086/592038](https://doi.org/10.1086/592038)